JOURNAL OF SPACECRAFT AND ROCKETS
Vol. 44, No. 2, March–April 2007

Sigma Point Filtering for Sequential Orbit Estimation and Prediction

Deok-Jin Lee* and Kyle T. Alfriend†
Texas A&M University, College Station, Texas 77843-3141

DOI: 10.2514/1.20702

The standard extended Kalman filter is widely used for nonlinear estimation. Its implementation, however, in orbit estimation under inaccurate initial conditions and sparse measurements can lead to unstable solutions. In this article, efficient alternatives to the extended Kalman filter are used for recursive nonlinear estimation of the states and parameter of an earth-orbiting satellite. The alternatives, called sigma point filters, include the unscented Kalman filter and the divided difference filter. The sigma point filters have advantages over the extended Kalman filter in that they do not require the burdensome derivation of the Jacobian and/or Hessian matrix, and they provide more accurate propagation of the state and error covariance matrix than those of the extended Kalman filter. An efficient filter initialization algorithm using the Herrick–Gibbs method is also proposed to provide an initial state and covariance. Simulation results indicate that the advantages of the sigma point filters make these attractive alternatives to the extended Kalman filter in the sequential orbit estimation with the same computational complexity of the extended Kalman filter.

Nomenclature

A	=	cross-sectional area
$\boldsymbol{a}_D$	=	atmospheric drag acceleration
$\boldsymbol{a}_G$	=	gravitational perturbation acceleration
B_C	=	ballistic coefficient
C_D	=	drag coefficient
E	=	expectation operator
$\boldsymbol{F}$	=	Jacobian of $\boldsymbol{f}$ with respect to the state $\boldsymbol{x}$
$\boldsymbol{f}$	=	state forcing function
$\mathcal{K}$	=	Kalman gain
m_s	=	satellite mass
$\mathcal{N}$	=	denotes normal or Gaussian distribution
n	=	dimension of state vector
n_a	=	dimension of augmented state vector
$\boldsymbol{P}$	=	covariance
$\boldsymbol{Q}$	=	process noise covariance
$\boldsymbol{R}$	=	measurement noise covariance
$\boldsymbol{R}_s$	=	radius from Earth center to sensor
$\boldsymbol{r}$	=	satellite position vector
t	=	time
$\boldsymbol{v}$	=	satellite velocity vector
$\boldsymbol{v}_k$	=	process noise
$\boldsymbol{v}_{\text{rel}}$	=	velocity relative to the atmosphere
$\boldsymbol{w}_k$	=	measurement noise vector
$\boldsymbol{x}$	=	state vector
$\tilde{\boldsymbol{y}}$	=	measurement vector
θ, ϕ	=	sensor latitude and longitude
μ	=	gravitational constant
$\boldsymbol{\upsilon}$	=	innovation vector
ρ	=	sensor to satellite range vector with components (ρ_u, ρ_e, ρ_n)
$\mathcal{X}^a_{i,k}$	=	sigma points

Received 23 October 2005; revision received 16 November 2006; accepted for publication 2 December 2006.

*Postdoctoral Research Associate, Department of Aerospace Engineering; djlee@aero.tamu.edu. Member AIAA.

†TEES Distinguished Research Chair Professor, Department of Aerospace Engineering; alfriend@aeromail.tamu.edu. Fellow AIAA.

I. Introduction

FOR the protection of the international space station (ISS) and other high-valued assets, an accurate estimate of the state and covariance of each space object in the space object catalog (SOC) is needed. Therefore, there is a need to track objects as small as 1–2 cm using ground-based sensor systems [1,2]. This would probably increase the space catalog size to 100,000–300,000 objects. Currently batch least-squares estimation is used for maintaining the space object catalog. The recursive nonlinear filters, such as the extended Kalman filter, should work equally as well. In both methods the dynamical system is linearized about the reference trajectory with the assumption that the deviation from the true state trajectory is small. This assumption makes the implementation of the recursive nonlinear filter feasible in nonlinear estimation problems. Because the reference trajectory in catalog maintenance is reasonably accurate, the linearization process is usually sufficient. However, one aspect of catalog maintenance in which an improved method would be useful is the cataloging of uncorrelated objects (UCOs). Each new object that enters the catalog begins as a UCO. These UCOs can be new objects or spacecrafts that have maneuvered, but primarily they are small space objects that are not tracked often enough to correlate the tracks and develop a sufficiently accurate element set. Many of them are only tracked when their attitude is advantageous for a sufficiently strong radar return. Consequently, the tracks may be widely separated and only sparse observations are available. From these tracks or observations a composite element set must be developed. Because the reference trajectory is just the initial track and the tracks can be widely separated, the linearization process used in the current batch least-squares estimator or the extended Kalman filter may lead to an inaccurate estimate and have difficulty in converging. An improved filter/estimator could play a major role in this area. If more widely separated tracks could be correlated and an element set developed, the cataloging process could be improved efficiently. To develop a catalog of 100,000 or more objects the correlation process will need to improve. The purpose of this paper is to investigate and use new nonlinear estimation algorithms for accurate sequential orbit determination of an earth-orbiting satellite or space object for catalog maintenance.

The extended Kalman filter (EKF) has been widely used for nonlinear estimation problems [3,4]. The filter works on the principle that the state distribution is approximated by a Gaussian random variable, and the state is propagated through the first-order linearization of the nonlinear equations. The series approximation can, however, introduce large errors in the true mean and covariance

of the posterior distribution, which can lead to biased suboptimal estimation, and even divergence of the filter [3]. In addition, the derivation of the Jacobian matrix is nontrivial in some systems. Even though the EKF theory has been a popular method for nonlinear estimation problems, its application in sequential orbit estimation under inaccurate a priori state and covariance values with widely separated short tracks can lead to an inaccurate estimate of the state of a satellite or space object. There are modification solutions to the problem in which the effects of the linearization of nonlinear systems can be compensated for by increasing the order of the Taylor-series expansion of the nonlinear system or by using an iterative technique, such as the iterated extended Kalman filter (IEKF) [3]. The modifications, however, only provide a partial solution rather than a complete solution, and increase the computational cost with a more complex implementation.

Recently, there have been interesting developments in derivative-free nonlinear estimation techniques as efficient alternatives to the EKF [4–8]. These methods include the unscented Kalman filter (UKF), the central difference filter (CDF), and the divided difference filter (DDF). We call them sigma point filters (SPFs) [9] in this paper. These novel methods are also called sigma point Kalman filters (SPKFs) [10]. The UKF [4,5], proposed by Julier et al., works on the principle that a set of deterministically sampled points, called sigma points, can be used to parameterize the mean and covariance of the Gaussian random variables, and the posterior mean and covariance are propagated through the true nonlinear function without the linearization step. The UKF is advantageous over the EKF in that 1) it can lead to a more accurate and stable estimate of the state and covariance, 2) the new filter can estimate with discontinuous functions, 3) no explicit derivation of the Jacobian and/or Hessian matrix is necessary, and 4) it is suitable for parallel processing. On the other hand, the CDF [6] and the DDF [7,8] adopt an alternative linearization method called the central difference approximation where derivatives are replaced by functional evaluations with a set of deterministically calculated sigma points, which leads to an easy expansion of the nonlinear functions to higher-order terms. This accommodates easy and efficient implementation of the filters in nonlinear estimation applications. Conceptually, the principles of two filters (the CDF and the DDF) resemble that of the EKF and its higher-order modifications. These two filters guarantee positive semidefiniteness of the posterior covariance, and are essentially identical to each other, thus they will be referred to jointly as the DDF in this paper. The expected theoretical performance of the DDF is at least similar, or even superior to that of the EKF, and is comparable to that of the modified second-order filter without the burdensome derivation of the Jacobian and/or Hessian matrix that is required by the EKF and its variants. Lee and Alfriend [11] empirically demonstrated in a systematic way that the overall performance of the UKF in the sequential orbit estimation application is superior to that of the EKF in the sense that the UKF is robust to the large initial errors and dynamic uncertainty. These advantages make the UKF suitable for application to some complex dynamic systems. In this paper, performance evaluation of the proposed sigma point nonlinear filters, along with the EKF, in terms of estimation accuracy and optimality is tested by applying these to the satellite orbit estimation in which sparse observational data from widely separated short-arc tracks are used. An efficient filter initialization algorithm using the Herrick–Gibbs [12] method is proposed to provide not only the initial state, but also covariance information that becomes the input to the recursive nonlinear filters.

The remainder of this paper is organized as follows: 1) review of filter system models, 2) a description of the formulation of the EKF algorithm, 3) formulation of the unscented Kalman filtering algorithm, 4) illustration of the formulation of the divided difference filter, 5) comparison of the performance of the proposed nonlinear filters, the EKF, UKF, and DDF in terms of estimation accuracy and optimality, and 6) discussion of the simulation results.

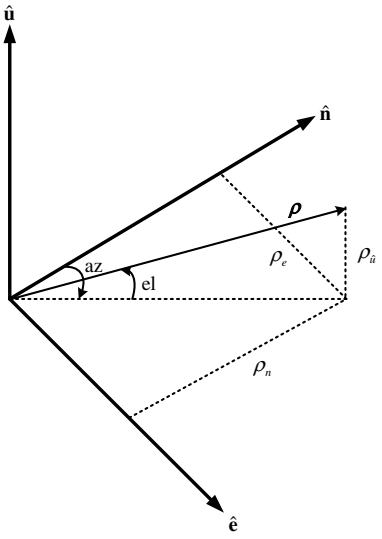

Fig. 1 Radar site coordinates for satellite observation.

II. Filtering System Model

A. Equations of Motion

The governing equations of motion for a near-Earth satellite in orbit are given by [12]

$$\dot{\boldsymbol{r}} = \boldsymbol{v} \qquad \dot{\boldsymbol{v}} = -\frac{\mu}{r^3}\boldsymbol{r} + \boldsymbol{a}_G + \boldsymbol{a}_D \tag{1}$$

With the initial conditions $\boldsymbol{r}(t_0)$ and $\boldsymbol{v}(t_0)$ at time t_0, a time history of the satellite's position and velocity is obtained. The instantaneous acceleration due to the atmospheric density is assumed to be opposed to the direction of motion and proportional to the atmospheric density ρ_d and the velocity squared.

$$\boldsymbol{a}_D = -\frac{1}{2B_C}\rho_d v_{\text{rel}}\boldsymbol{v}_{\text{rel}} \tag{2}$$

$$B_C = \frac{m_s}{C_d A} \tag{3}$$

B. Measurement Model

The inertial position vector has the relation with the range vector and the radar site vector [12]

$$\boldsymbol{r} = \boldsymbol{R}_s + \rho \tag{4}$$

where $\boldsymbol{r} = [x, y, z]^T$. The range vector ρ from the radar site shown in Fig. 1 is described in terms of the "zenith," "east," and "north" coordinates:

$$\rho = \rho_u\hat{\boldsymbol{u}} + \rho_e\hat{\boldsymbol{e}} + \rho_n\hat{\boldsymbol{n}} \tag{5}$$

The range is obtained by

$$\rho = \sqrt{\rho_u^2 + \rho_e^2 + \rho_n^2} \tag{6}$$

The azimuth (az) and elevation (el) angles are expressed by

$$\text{az} = \tan^{-1}\left(\frac{\rho_e}{\rho_n}\right) \tag{7}$$

$$\text{el} = \tan^{-1}\left(\frac{\rho_u}{\sqrt{\rho_e^2 + \rho_n^2}}\right) \tag{8}$$

The components of the range vector in terms of the inertial position, and sensor radius, longitude, and latitude are

$$\begin{aligned}\rho_u &= \cos\phi\cos\theta[x - R_s\cos\phi\cos\theta] + \cos\phi\sin\theta[y \\ &\quad - R_s\cos\phi\sin\theta] + \sin\phi[z - R_s\sin\phi] \\ \rho_e &= -\sin\theta[x - R_s\cos\phi\cos\theta] + \cos\theta[y - R_s\cos\phi\sin\theta] \\ \rho_n &= -\sin\phi\cos\theta[x - R_s\cos\phi\cos\theta] - \sin\phi\sin\theta[y \\ &\quad - R_s\cos\phi\sin\theta] + \cos\phi[z - R_s\sin\phi]\end{aligned} \tag{9}$$

III. Extended Kalman Filter

The extended Kalman filter provides the minimum variance estimate of the state based on statistical information about the dynamical and observation models. The continuous-time models can be converted into a discrete form through an approximate method [3]. In this section the EKF algorithm is reviewed for discrete-time nonlinear equations of the form

$$\boldsymbol{x}_{k+1} = \boldsymbol{f}(\boldsymbol{x}_k, \boldsymbol{w}_k, k) \tag{10}$$

$$\tilde{\boldsymbol{y}}_k = \boldsymbol{h}(\boldsymbol{x}_k, \boldsymbol{v}_k, k) \tag{11}$$

where $\boldsymbol{x}_k \in \Re^n$ is the $n \times 1$ state vector, $\tilde{\boldsymbol{y}} \in \Re^m$ is the $m \times 1$ observation vector, $\boldsymbol{w}_k \in \Re^q$ is the $q \times 1$ state noise vector, and $\boldsymbol{v}_k \in \Re^l$ is the $l \times 1$ measurement noise vector. It is assumed that the noise vectors are zero-mean Gaussian processes satisfying

$$\begin{gathered}E\left\{\boldsymbol{w}_k\boldsymbol{w}_j^T\right\} = \delta_{kj}\boldsymbol{Q}_k, \qquad E\left\{\boldsymbol{v}_k\boldsymbol{v}_j^T\right\} = \delta_{kj}\boldsymbol{R}_k \\ E\left\{\boldsymbol{v}_k\boldsymbol{w}_j^T\right\} = 0, \quad \forall\ k, j\end{gathered} \tag{12}$$

where the noise covariances $\boldsymbol{Q}_k$ and $\boldsymbol{R}_k$ are assumed to be positive definite. Given a system model with initial state and covariance values, the EKF propagates the state vector and the error covariance matrix recursively. Then, along with imperfect measurements, the EKF updates the state and covariance matrix. The update is accomplished through the Kalman gain matrix $\mathcal{K}$, which is obtained by minimizing the weighted sum of the diagonal elements of the error covariance matrix. Thus, the EKF algorithm has a distinctive predictor–corrector structure. The prediction phase is important for overall filter performance. The EKF is based on the linearization by using the Taylor-series expansion of the nonlinear dynamical and measurement equations about the current estimate. For the nonlinear models in Eqs. (10) and (11) the predictions of the state estimates and covariance are accomplished by

$$\hat{\boldsymbol{x}}_{k+1}^- = \boldsymbol{f}(\hat{\boldsymbol{x}}_k, k) \tag{13}$$

$$\boldsymbol{P}_{k+1}^- = \boldsymbol{F}_k\boldsymbol{P}_k\boldsymbol{F}_k^T + \boldsymbol{Q}_k \tag{14}$$

where $\boldsymbol{F}_k$ is the Jacobian matrix of the nonlinear function $\boldsymbol{f}(\cdot,\cdot)$ evaluated about the current state $\hat{\boldsymbol{x}}_k \equiv \hat{\boldsymbol{x}}_k^+$. The update equation can be expressed by

$$\hat{\boldsymbol{x}}_{k+1}^+ = \hat{\boldsymbol{x}}_{k+1}^- + \mathcal{K}_{k+1}\boldsymbol{\upsilon}_{k+1} \tag{15}$$

$$\boldsymbol{P}_{k+1}^+ = \boldsymbol{P}_{k+1}^- - \mathcal{K}_{k+1}\boldsymbol{P}_{k+1}^{\upsilon\upsilon}\mathcal{K}_{k+1}^T \tag{16}$$

where the innovation vector $\boldsymbol{\upsilon}_{k+1}$ is equal to the difference between the actual and the predicted observations:

$$\boldsymbol{\upsilon}_{k+1} \equiv \tilde{\boldsymbol{y}}_{k+1} - \hat{\boldsymbol{y}}_{k+1}^- = \tilde{\boldsymbol{y}}_{k+1} - \boldsymbol{h}(\hat{\boldsymbol{x}}_{k+1}^-, k+1) \tag{17}$$

The covariance of the innovation vector is obtained by

$$\boldsymbol{P}_{k+1}^{\upsilon\upsilon} = \boldsymbol{P}_{k+1}^{yy} + \boldsymbol{R}_{k+1} = \boldsymbol{H}_{k+1}\boldsymbol{P}_{k+1}^-\boldsymbol{H}_{k+1}^T + \boldsymbol{R}_{k+1} \tag{18}$$

where $\boldsymbol{P}_{k+1}^{yy} = \boldsymbol{H}_{k+1}\boldsymbol{P}_{k+1}^-\boldsymbol{H}_{k+1}^T$ is the output covariance matrix, and $\boldsymbol{H}_{k+1}$ is the Jacobian matrix of the nonlinear measurement function $\boldsymbol{h}(\cdot,\cdot)$ evaluated about the predicted state $\hat{\boldsymbol{x}}_{k+1}^-$. Now, the Kalman gain $\mathcal{K}_{k+1}$ is computed by

$$\mathcal{K}_{k+1} = \boldsymbol{P}_{k+1}^{xy}\left(\boldsymbol{P}_{k+1}^{\upsilon\upsilon}\right)^{-1} \tag{19}$$

where $\boldsymbol{P}_{k+1}^{xy} = \boldsymbol{P}_{k+1}^-\boldsymbol{H}_{k+1}^T$ is the predicted cross-correlation matrix between the predicted state $\hat{\boldsymbol{x}}_{k+1}^-$ and measurement $\hat{\boldsymbol{y}}_{k+1}^-$. Note that in the EKF algorithm the state distribution is approximated by a Gaussian random variable, which is then propagated through the first-order linearization of the nonlinear functions. These approximations, however, can introduce large errors in the true posterior mean and covariance. The SPFs use different prediction approaches that are discussed in the next section.

IV. Sigma Point Filtering

The common procedures of the sigma point filtering approach can be described with three steps. First, a set of weighted sigma points are deterministically calculated by applying a specific sampling approach such as the unscented transformation for the UKF and the central transformation for the DDF. Then, the sampled sigma points are propagated through the true nonlinear function. Finally, the posterior statistics, mean and covariance, are computed by using either a statistical linear regression or tractable functional evaluations with the propagated sigma points. The algorithms of the UKF and DDF are formulated after taking the aforementioned sigma point filtering steps.

A. Unscented Kalman Filter

The basic difference between the extended Kalman filter [3] and the unscented Kalman filter [5] results from the manner in which the state distribution of the nonlinear models is approximated. The unscented Kalman filter (UKF), introduced by Julier et al. [4,5], uses a nonlinear transformation, called the scaled unscented transformation (SUT), in which the state probability distribution is represented by a set of weighted sigma points, and they are used to parameterize the true mean and covariance of the state distribution. When the sigma points are propagated through the true nonlinear systems, the posterior mean and covariance is obtained up to the second order for any nonlinearity. The unscented Kalman filter algorithm is summarized in this section for the discrete-time nonlinear models in Eqs. (10) and (11). See [5] for details.

The original state vector is redefined as an augmented state vector along with noise variables and the augmented covariance matrix on the diagonal is reconstructed by

$$\boldsymbol{x}_k^a = \begin{bmatrix}\boldsymbol{x}_k \\ \boldsymbol{w}_k \\ \boldsymbol{v}_k\end{bmatrix}, \qquad \boldsymbol{P}_k^a = \begin{bmatrix}\boldsymbol{P}_k & \boldsymbol{0} & \boldsymbol{0} \\ \boldsymbol{0} & \boldsymbol{Q}_k & 0 \\ \boldsymbol{0} & \boldsymbol{0} & \boldsymbol{R}_k\end{bmatrix} \tag{20}$$

where $\boldsymbol{x}_k^a \in \Re^{n_a}$ is the augmented state vector with the dimension $n_a = n + q + l$. Then, the set of scaled symmetric sigma points $\{\mathcal{X}_{i,k}^a\}_{i=0}^{2n_a} = \{[(\mathcal{X}_{i,k}^x)^T(\mathcal{X}_{i,k}^w)^T(\mathcal{X}_{i,k}^v)^T]^T\}_{i=0}^{2n_a}$ with the augmented state vector and covariance matrix is constructed by

$$\begin{gathered}\mathcal{X}_{0,k}^a = \hat{\boldsymbol{x}}_k^a \qquad \mathcal{X}_{i,k}^a = \hat{\boldsymbol{x}}_k^a + [\sqrt{(n_a+\lambda)\boldsymbol{P}_k^a}]_i, \qquad i = 1,\ldots,n_a \\ \mathcal{X}_{i,k}^a = \hat{\boldsymbol{x}}_k^a - [\sqrt{(n_a+\lambda)\boldsymbol{P}_k^a}]_i, \qquad i = n_a+1,\ldots,2n_a\end{gathered} \tag{21}$$

where $\lambda = \alpha^2(n_a + \kappa) - n_a$ includes scaling parameters. The constant parameter α controls the size of the sigma point distribution and should be a small number $0 \le \alpha \le 1$, and κ provides an extra degree of freedom that is used to fine-tune the higher-order moments; $\kappa = 3 - n_a$ for a Gaussian distribution [13]. $[\sqrt{(n_a+\lambda)\boldsymbol{P}_k^a}]_i$ is the ith column or row vector of the weighted square root of the scaled covariance matrix $(n_a + \lambda)\boldsymbol{P}_k^a$.

As for the state propagation step, the predicted state vector $\hat{\boldsymbol{x}}_{k+1}^-$ and its predicted covariance $\boldsymbol{P}_{k+1}^-$ are computed using the propagated sigma point vectors

$$\mathcal{X}^{x}_{k+1} = \boldsymbol{f}\left(\mathcal{X}^{x}_{k}, \mathcal{X}^{w}_{k}, k\right) \tag{22}$$

$$\hat{\boldsymbol{x}}^{-}_{k+1} = \sum_{i=0}^{2n_a} W_i^{(m)} \mathcal{X}^{x}_{i,k+1} \tag{23}$$

$$\boldsymbol{P}^{-}_{k+1} = \sum_{i=0}^{2n_a} W_i^{(c)} [\mathcal{X}^{x}_{i,k+1} - \hat{\boldsymbol{x}}^{-}_{k+1}][\mathcal{X}^{x}_{i,k+1} - \hat{\boldsymbol{x}}^{-}_{k+1}]^T \tag{24}$$

where $\mathcal{X}^{x}_{i,k}$ is a weighted sigma point vector of the first n elements of the ith augmented sigma point vector $\mathcal{X}^{a}_{i,k}$ and $\mathcal{X}^{w}_{i,k}$ is a weighted sigma point vector of the next q elements of $\mathcal{X}^{a}_{i,k}$, respectively. Similarly, the predicted observation vector $\hat{\boldsymbol{y}}^{-}_{k+1}$ and the innovation covariance $\boldsymbol{P}^{vv}_{k+1}$ are calculated

$$\mathcal{Y}_{k+1} = \boldsymbol{h}\left(\mathcal{X}^{x}_{k+1}, \mathcal{X}^{v}_{k+1}, k+1\right) \tag{25}$$

$$\hat{\boldsymbol{y}}^{-}_{k+1} = \sum_{i=0}^{2n_a} W_i^{(m)} \mathcal{Y}_{i,k+1} \tag{26}$$

$$\boldsymbol{P}^{vv}_{k+1} = \sum_{i=0}^{2n_a} W_i^{(c)} [\mathcal{Y}_{i,k+1} - \hat{\boldsymbol{y}}^{-}_{k+1}][\mathcal{Y}_{i,k+1} - \hat{\boldsymbol{y}}^{-}_{k+1}]^T \tag{27}$$

where $\mathcal{X}^{v}_{i,k}$ is a weighted sigma point vector of the l elements of the ith augmented sigma point vector $\mathcal{X}^{a}_{i,k}$, and $W_i^{(m)}$ is the weight for the mean and $W_i^{(c)}$ is the weight for the covariance, respectively:

$$\begin{aligned} W_i^{(m)} &= \begin{cases} \lambda/(n_a+\lambda) & i=0 \\ 1/\{2(n_a+\lambda)\} & i=1,\ldots,2n_a \end{cases} \\ W_i^{(c)} &= \begin{cases} \lambda/(n_a+\lambda) + (1-\alpha^2+\beta) & i=0 \\ 1/\{2(n_a+\lambda)\} & i=1,\ldots,2n_a \end{cases} \end{aligned} \tag{28}$$

where β is a third parameter that further incorporates higher-order effects by adding the weighting of the zeroth sigma point to the calculation of the covariance, and $\beta = 2$ is the optimal value for Gaussian distributions [5]. Now, the filter gain $\mathcal{K}_{k+1}$ is computed by

$$\mathcal{K}_{k+1} = \boldsymbol{P}^{xy}_{k+1} (\boldsymbol{P}^{\upsilon\upsilon}_{k+1})^{-1} \tag{29}$$

and the cross-correlation matrix is determined by

$$\boldsymbol{P}^{xy}_{k+1} = \sum_{i=0}^{2n_a} W_i^{(c)} \left\{\mathcal{X}^{x}_{i,k+1} - \hat{\boldsymbol{x}}^{-}_{k+1}\right\}\left\{\mathcal{Y}_{i,k+1} - \hat{\boldsymbol{y}}^{-}_{k+1}\right\}^T \tag{30}$$

The estimated state vector $\hat{\boldsymbol{x}}^{+}_{k+1}$ and updated covariance $\boldsymbol{P}^{+}_{k+1}$ are given by

$$\hat{\boldsymbol{x}}^{+}_{k+1} = \hat{\boldsymbol{x}}^{-}_{k+1} + \mathcal{K}_{k+1}\boldsymbol{\upsilon}_{k+1} \tag{31}$$

$$\boldsymbol{P}^{+}_{k+1} = \boldsymbol{P}^{-}_{k+1} - \mathcal{K}_{k+1}\boldsymbol{P}^{vv}_{k+1}\mathcal{K}^{T}_{k+1} \tag{32}$$

It is noted that in the formulation of the UKF algorithm the correlated noise sources can be implemented efficiently without any modification of the filter algorithm. For the special case where both the process and measurement noises are purely additive, the computational complexity of the UKF can be reduced by adjusting the augmented state vector [11,13]. For the computational stability the matrix square root can be implemented by using a Cholesky factorization method that prevents the nonnegative covariance matrix [13].

B. Divided Difference Filter

In this section, the divided difference filter proposed by Norgaard et al. [7] is introduced as an efficient extension of the extended Kalman filter for nonlinear systems. As described in the UKF algorithm the DDF can be also described as a sigma point filter in that the filter linearizes the nonlinear dynamic and measurement functions by using an interpolation formula through systematically chosen $2n$ sigma points. The linearization is based on polynomial approximations of the nonlinear transformations that are obtained by Stirling's interpolation formula, rather than the partial derivative based Taylor-series approximation. Conceptually, the implementation of the DDF resembles that of the EKF. The implementation, however, is significantly simpler because it is not necessary to formulate the Jacobian and/or Hessian matrices of the partial derivatives of the nonlinear dynamic and measurement equations. Thus, the new nonlinear filter can also replace the extended Kalman filter and its higher-order variants in practical real-time applications that require accurate estimation, but with less computational cost. In this section, the DDF algorithm is formulated by using the second-order divided difference approximation of the nonlinear equations in terms of the innovation vector approach and a set of scaled sigma points.

Consider the general discrete-time nonlinear models in Eqs. (10) and (11) with the assumption that the noise vectors are uncorrelated white Gaussian processes with unknown expected mean and covariances

$$\boldsymbol{w}_k: \mathcal{N}(\bar{\boldsymbol{w}}_k, \boldsymbol{Q}_k), \qquad \boldsymbol{v}_k: \mathcal{N}(\bar{\boldsymbol{v}}_k, \boldsymbol{R}_k) \tag{33}$$

First, the square-root Cholesky factorizations are introduced:

$$\boldsymbol{P}_k = \boldsymbol{S}_{\boldsymbol{x},k}\boldsymbol{S}^T_{\boldsymbol{x},k}, \qquad \boldsymbol{Q}_k = \boldsymbol{S}_{\boldsymbol{w},k}\boldsymbol{S}^T_{\boldsymbol{w},k} \tag{34}$$

Now, the augmented state vector $\hat{\boldsymbol{x}}^{xw}_k \in \Re^{n_{xw}}$ and the augmented square-root matrix $\boldsymbol{S}^{xw}_k \in \Re^{n_{xw}\times n_{xw}}$ are constructed by

$$\hat{\boldsymbol{x}}^{xw}_k = \begin{bmatrix} \hat{\boldsymbol{x}}_k \\ \bar{\boldsymbol{w}}_k \end{bmatrix}, \qquad \boldsymbol{S}^{xw}_k = \begin{bmatrix} \boldsymbol{S}_{\boldsymbol{x},k} & \boldsymbol{0} \\ \boldsymbol{0} & \boldsymbol{S}_{\boldsymbol{w},k} \end{bmatrix} \tag{35}$$

where the dimension n_{xw} of the augmented state vector $\hat{\boldsymbol{x}}^{xw}_k$ is the sum of the dimension n_x of the state vector and the dimension n_w of process noise vector, $n_{xw} = n_x + n_w$. Then, the set of scaled symmetric sigma points $\{\mathcal{X}^{xw}_{i,k}\}_{i=0}^{2n_{xw}}$ is constructed by

$$\begin{aligned} \mathcal{X}^{xw}_{0,k} &= \hat{\boldsymbol{x}}^{xw}_k \qquad \mathcal{X}^{xw}_{i,k} = \hat{\boldsymbol{x}}^{xw}_k + h\boldsymbol{S}^{xw}_{i,k}, \qquad i = 1,\ldots,n_{xw} \\ &\qquad \mathcal{X}^{xw}_{i,k} = \hat{\boldsymbol{x}}^{xw}_k - h\boldsymbol{S}^{xw}_{i,k}, \qquad i = n_{xw}+1,\ldots,2n_{xw} \end{aligned} \tag{36}$$

where $\boldsymbol{S}^{xw}_{i,k}$ is the ith sigma point column vector of $\boldsymbol{S}^{xw}_k$ given from Eq. (35) and h is a scaling weight factor coming from the divided difference interval size [8]. The predicted state vector $\hat{\boldsymbol{x}}^{-}_{k+1}$ is computed by using the constructed sigma points $\mathcal{X}^{xw}_{i,k}$:

$$\hat{\boldsymbol{x}}^{-}_{k+1} = W^{(m)}_{d,0}\boldsymbol{f}\left(\mathcal{X}^{x}_{0,k}, \mathcal{X}^{w}_{0,k}\right) + W^{(m)}_{d,1}\sum_{i=1}^{2n_{xw}} \boldsymbol{f}\left(\mathcal{X}^{x}_{i,k}, \mathcal{X}^{w}_{i,k}\right) \tag{37}$$

where the weight parameters have the values $W^{(m)}_{d,0} = h^2 - (n_x + n_w)/h^2$ and $W^{(m)}_{d,1} = 1/2h^2$, and $\mathcal{X}^{x}_{i,k}$ is a weighted sigma point vector of the first n_x elements of the ith augmented sigma point vector $\mathcal{X}^{xw}_{i,k}$ and $\mathcal{X}^{w}_{i,k}$ is a weighted sigma point vector of the next n_w elements of $\mathcal{X}^{xw}_{i,k}$, respectively. Van der Merwe et al. [10] showed that the second-order prediction accuracy of the state estimate is identical to that of the UKF. The predicted state covariance matrix $\boldsymbol{P}^{-}_{k+1}$ is computed by

$$\boldsymbol{P}^{-}_{k+1} = \mathcal{S}^{-}_{\boldsymbol{x}}(k+1)[\mathcal{S}^{-}_{\boldsymbol{x}}(k+1)]^T \tag{38}$$

where $\mathcal{S}^{-}_{\boldsymbol{x}}(k+1) \in \Re^{n_x\times 2n_{xw}}$ is the state compound matrix

$$\begin{aligned} &\mathcal{S}^{-}_{\boldsymbol{x}}(k+1) \\ &\quad = [\,\boldsymbol{S}^{(1)}_{\boldsymbol{x}\hat{\boldsymbol{x}}}(k+1) \quad \boldsymbol{S}^{(1)}_{\boldsymbol{x}\boldsymbol{w}}(k+1) \quad \boldsymbol{S}^{(2)}_{\boldsymbol{x}\hat{\boldsymbol{x}}}(k+1) \quad \boldsymbol{S}^{(2)}_{\boldsymbol{x}\boldsymbol{w}}(k+1)\,] \end{aligned} \tag{39}$$

and each component matrix of the state compound matrix is given by

$$
\begin{aligned}
&\boldsymbol{S}^{(1)}_{\boldsymbol{x}\hat{\boldsymbol{x}},i}(k+1) = W^{(c)}_{d,1}\Big[\boldsymbol{f}\Big(\mathcal{X}^{x}_{i,k},\mathcal{X}^{w}_{0,k}\Big) - \boldsymbol{f}\Big(\mathcal{X}^{x}_{i+n_{xw},k},\mathcal{X}^{w}_{0,k}\Big)\Big]\\
&i = 1,\ldots,n_x\\
&\boldsymbol{S}^{(1)}_{\boldsymbol{x}\boldsymbol{w},i}(k+1) = W^{(c)}_{d,1}\Big[\boldsymbol{f}\Big(\mathcal{X}^{x}_{0,k},\mathcal{X}^{w}_{i+n_x,k}\Big) - \boldsymbol{f}(\mathcal{X}^{x}_{0,k},\mathcal{X}^{w}_{i+n_{xw}+n_x,k}\Big)\Big]\\
&i = 1,\ldots,n_w\\
&\boldsymbol{S}^{(2)}_{\boldsymbol{x}\hat{\boldsymbol{x}},i}(k+1) = W^{(c)}_{d,2}\Big[\boldsymbol{f}\Big(\mathcal{X}^{x}_{i,k},\mathcal{X}^{w}_{0,k}\Big) + \boldsymbol{f}\Big(\mathcal{X}^{x}_{i+n_{xw},k},\mathcal{X}^{w}_{0,k}\Big)\\
&\quad - 2\boldsymbol{f}\Big(\mathcal{X}^{x}_{0,k},\mathcal{X}^{w}_{0,k}\Big)\Big]\\
&i = 1,\ldots,n_x\\
&\boldsymbol{S}^{(2)}_{\boldsymbol{x}\boldsymbol{w},i}(k+1) = W^{(c)}_{d,2}\Big[\boldsymbol{f}\Big(\mathcal{X}^{x}_{0,k},\mathcal{X}^{w}_{i+n_x,k}\Big) + \boldsymbol{f}\Big(\mathcal{X}^{x}_{0,k},\mathcal{X}^{w}_{i+n_{xw}+n_x,k}\Big)\\
&\quad - 2\boldsymbol{f}\Big(\mathcal{X}^{x}_{0,k},\mathcal{X}^{w}_{0,k}\Big)\Big]\\
&i = 1,\ldots,n_w
\end{aligned}
\tag{40}
$$

where $W^{(c)}_{d,1} = 1/2h$ and $W^{(c)}_{d,2} = \sqrt{h^2-1}/2h^2$. $\boldsymbol{S}^{(1)}_{\boldsymbol{x}\hat{\boldsymbol{x}},i}$ and $\boldsymbol{S}^{(2)}_{\boldsymbol{x}\hat{\boldsymbol{x}},i}$ is the ith column vector of each component matrix $\boldsymbol{S}^{(1)}_{\boldsymbol{x}\hat{\boldsymbol{x}}} \in \Re^{n_x\times n_x}$ and $\boldsymbol{S}^{(2)}_{\boldsymbol{x}\hat{\boldsymbol{x}}} \in \Re^{n_x\times n_x}$, and $\boldsymbol{S}^{(1)}_{\boldsymbol{x}\boldsymbol{w},i}$ and $\boldsymbol{S}^{(2)}_{\boldsymbol{x}\boldsymbol{w},i}$ is the ith column vector of each component matrix $\boldsymbol{S}^{(1)}_{\boldsymbol{x}\boldsymbol{w}} \in \Re^{n_x\times n_w}$ and $\boldsymbol{S}^{(2)}_{\boldsymbol{x}\boldsymbol{w}} \in \Re^{n_x\times n_w}$, respectively. Theoretically, it is also proved that the accuracy of the covariance prediction is close to that of the UKF (see [8] for details). For the measurement update, the augmented state vector $\hat{\boldsymbol{x}}^{xv}_{k+1} \in \Re^{n_{xv}}$ and the augmented square-root matrix $\boldsymbol{S}^{xv}_{k+1} \in \Re^{n_{xv}\times n_{xv}}$ are constructed by

$$
\hat{\boldsymbol{x}}^{\,xv}_{k+1} = \begin{bmatrix} \hat{\boldsymbol{x}}^{-}_{k+1} \\ \bar{\boldsymbol{v}}_{k+1} \end{bmatrix}, \qquad \boldsymbol{S}^{xv}_{k+1} = \begin{bmatrix} \boldsymbol{S}^{-}_{\boldsymbol{x},k+1} & \boldsymbol{0} \\ \boldsymbol{0} & \boldsymbol{S}_{\boldsymbol{v},k+1} \end{bmatrix} \tag{41}
$$

where the dimension n_{xv} of the augmented state vector $\hat{\boldsymbol{x}}^{xv}_{k+1}$ is the sum of the dimension n_x of the state vector and the dimension n_v of measurement noise vector, $n_{xv} = n_x + n_v$. $\boldsymbol{S}^{-}_{\boldsymbol{x},k+1}$ and $\boldsymbol{S}_{\boldsymbol{v},k+1}$ are the square-root matrices obtained from the Cholesky factorization of the predicted state covariance and the measurement noise covariance,

$$
\boldsymbol{P}^{-}_{k+1} = \boldsymbol{S}^{-}_{\boldsymbol{x},k+1}(\boldsymbol{S}^{-}_{\boldsymbol{x},k+1})^T, \qquad \boldsymbol{R}_{k+1} = \boldsymbol{S}_{\boldsymbol{v},k+1}\boldsymbol{S}^{T}_{\boldsymbol{v},k+1} \tag{42}
$$

Now, the set of scaled symmetric sigma points $\{\mathcal{X}^{xv}_{i,k+1}\}^{2n_{xv}}_{i=0}$ for the measurement update is constructed by

$$
\begin{aligned}
\mathcal{X}^{\,xv}_{0,k+1} = \hat{\boldsymbol{x}}^{xv}_{k+1} \qquad \mathcal{X}^{xv}_{i,k+1} = \hat{\boldsymbol{x}}^{xv}_{k+1} + h\boldsymbol{S}^{xv}_{i,k+1}, \qquad i = 1,\ldots,n_{xv}\\
\mathcal{X}^{xv}_{i,k+1} = \hat{\boldsymbol{x}}^{xv}_{k+1} - h\boldsymbol{S}^{xv}_{i,k+1}, \qquad i = n_{xv}+1,\ldots,2n_{xv}
\end{aligned}
\tag{43}
$$

where $\boldsymbol{S}^{xv}_{i,k+1}$ is the ith sigma point column vector of $\boldsymbol{S}^{xv}_{k+1}$ in Eq. (41). Then, the predicted observation vector $\hat{\boldsymbol{y}}^{-}_{k+1} \in \Re^{n_y}$ is computed by

$$
\hat{\boldsymbol{y}}^{\,-}_{k+1} = W^{(m)}_{d,2}\boldsymbol{h}\Big(\mathcal{X}^{x}_{0,k+1},\mathcal{X}^{v}_{0,k+1}\Big) + W^{(m)}_{d,1}\sum_{i=1}^{2n_{xv}}\boldsymbol{h}\Big(\mathcal{X}^{x}_{i,k+1},\mathcal{X}^{v}_{i,k+1}\Big) \tag{44}
$$

where $W^{(m)}_{d,2}$ is the scale weight factor having the value $W^{(m)}_{d,2} = h^2 - (n_x+n_v)/h^2$. The innovation covariance matrix is formulated by

$$
\boldsymbol{P}^{\,vv}_{k+1} = \mathcal{S}_{\upsilon}(k+1)\mathcal{S}^{T}_{\upsilon}(k+1) \tag{45}
$$

where $\mathcal{S}_{\upsilon}(k+1) \in \Re^{n_y\times 2n_{xv}}$ is the innovation compound matrix

$$
\begin{aligned}
\mathcal{S}_{\upsilon}(k+1) = \Big[&\boldsymbol{S}^{(1)}_{\boldsymbol{y}\hat{\boldsymbol{x}}}(k+1) \qquad \boldsymbol{S}^{(1)}_{\boldsymbol{y}\boldsymbol{v}}(k+1) \qquad \boldsymbol{S}^{(2)}_{\boldsymbol{y}\hat{\boldsymbol{x}}}(k+1)\\
&\boldsymbol{S}^{(2)}_{\boldsymbol{y}\boldsymbol{v}}(k+1)\Big]
\end{aligned}
\tag{46}
$$

and each component matrix consisting the innovation compound matrix is given by

$$
\begin{aligned}
&\boldsymbol{S}^{(1)}_{\boldsymbol{y}\hat{\boldsymbol{x}},i}(k+1) = W^{(c)}_{d,1}\Big[\boldsymbol{h}\Big(\mathcal{X}^{x}_{i,k+1},\mathcal{X}^{v}_{0,k+1}\Big) - \boldsymbol{h}\Big(\mathcal{X}^{x}_{i+n_{xv},k+1},\mathcal{X}^{v}_{0,k+1}\Big)\Big]\\
&i = 1,\ldots,n_x\\
&\boldsymbol{S}^{(1)}_{\boldsymbol{y}\boldsymbol{v},i}(k+1) = W^{(c)}_{d,1}\Big[\boldsymbol{h}\Big(\mathcal{X}^{x}_{0,k+1},\mathcal{X}^{v}_{i+n_x,k+1}\Big)\\
&\quad - \boldsymbol{h}\Big(\mathcal{X}^{x}_{0,k+1},\mathcal{X}^{v}_{i+n_{xv}+n_x,k+1}\Big)\Big]\\
&i = 1,\ldots,n_v\\
&\boldsymbol{S}^{(2)}_{\boldsymbol{y}\hat{\boldsymbol{x}},i}(k+1) = W^{(c)}_{d,2}\Big[\boldsymbol{h}\Big(\mathcal{X}^{x}_{i,k+1},\mathcal{X}^{v}_{0,k+1}\Big) + \boldsymbol{h}\Big(\mathcal{X}^{x}_{i+n_{xv},k+1},\mathcal{X}^{v}_{0,k+1}\Big)\\
&\quad - 2\boldsymbol{h}\Big(\mathcal{X}^{x}_{0,k+1},\mathcal{X}^{v}_{0,k+1}\Big)\Big]\\
&i = 1,\ldots,n_x\\
&\boldsymbol{S}^{(2)}_{\boldsymbol{y}\boldsymbol{v},i}(k+1) = W^{(c)}_{d,2}\Big[\boldsymbol{h}\Big(\mathcal{X}^{x}_{0,k+1},\mathcal{X}^{v}_{i+n_x,k+1}\Big)\\
&\quad + \boldsymbol{h}\Big(\mathcal{X}^{x}_{0,k+1},\mathcal{X}^{v}_{i+n_{xv}+n_x,k+1}\Big) - 2\boldsymbol{h}\Big(\mathcal{X}^{x}_{0,k+1},\mathcal{X}^{v}_{0,k+1}\Big)\Big]\\
&i = 1,\ldots,n_v
\end{aligned}
\tag{47}
$$

where $\boldsymbol{S}^{(1)}_{\boldsymbol{y}\hat{\boldsymbol{x}},i}$ and $\boldsymbol{S}^{(2)}_{\boldsymbol{y}\hat{\boldsymbol{x}},i}$ is the ith column vector of each component matrix of $\boldsymbol{S}^{(1)}_{\boldsymbol{y}\hat{\boldsymbol{x}}} \in \Re^{n_y\times n_x}$ and $\boldsymbol{S}^{(2)}_{\boldsymbol{y}\hat{\boldsymbol{x}}} \in \Re^{n_y\times n_x}$, and also $\boldsymbol{S}^{(1)}_{\boldsymbol{y}\boldsymbol{v},i}$ and $\boldsymbol{S}^{(2)}_{\boldsymbol{y}\boldsymbol{v},i}$ is the ith column vector of each component matrix of $\boldsymbol{S}^{(1)}_{\boldsymbol{y}\boldsymbol{v}} \in \Re^{n_y\times n_v}$ and $\boldsymbol{S}^{(2)}_{\boldsymbol{y}\boldsymbol{v}} \in \Re^{n_y\times n_v}$, respectively. Similarly, the cross-correlation matrix is calculated by

$$
\boldsymbol{P}^{\,xy}_{k+1} = \mathcal{S}^{-}_{\boldsymbol{x}}(k+1)[\boldsymbol{S}^{(1)}_{\boldsymbol{y}\hat{\boldsymbol{x}}}(k+1)]^T \tag{48}
$$

Now, the filter gain matrix $\mathcal{K}_{k+1}$ is computed by

$$
\mathcal{K}_{\,k+1} = \boldsymbol{P}^{xy}_{k+1}\Big(\boldsymbol{P}^{\upsilon\upsilon}_{k+1}\Big)^{-1} \tag{49}
$$

Finally, the estimated state vector $\hat{\boldsymbol{x}}^{+}_{k+1}$ and updated covariance $\boldsymbol{P}^{+}_{k+1}$ are given by using the same formulas expressed in Eqs. (31) and (32), respectively.

V. Filter Initialization for Orbit Estimation

In catalog maintenance uncorrelated objects can be just-launched objects or satellites that have maneuvered, but often they are small space objects that are not tracked often enough to correlate the tracks and develop a sufficiently accurate element set. Many of them are only tracked when their attitude is advantageous for a sufficiently strong radar return. Consequently, the tracks are widely separated and may only be occasionally detected. In these cases the reference trajectory used for estimation is just the initial track. In satellite trajectory estimation applications, a batch filter can be used to enhance the covariance matrix fidelity and error convergence by providing an initial state estimate and covariance matrix [14]. The batch initialization, however, is not usually available when trying to correlate uncorrelated tracks because the reference trajectory is just the initial track and the tracks can be widely separated. Thus for establishing accurate estimate conditions a few measurements are used to produce an initial guess of the state and covariance. In this paper, the Herrick–Gibbs (HG) algorithm [12] is used to generate the initial state estimates, which are inputs for the recursive nonlinear filters. Figure 2 depicts the procedure of how to generate the desired information.

A typical ground-based sensor site's observation of a pass by a satellite usually results in many observations. The Herrick–Gibbs method is useful particularly when the observations are close together (short-arc observations) and provides velocity information from three position vectors $(\boldsymbol{r}_1, \boldsymbol{r}_2, \boldsymbol{r}_3)$. Suppose the location of the sensor is known in terms of the longitude θ and latitude ϕ. Then using three observations consisting of range, azimuth, and elevation, the position vectors are calculated at the time of each observation. The

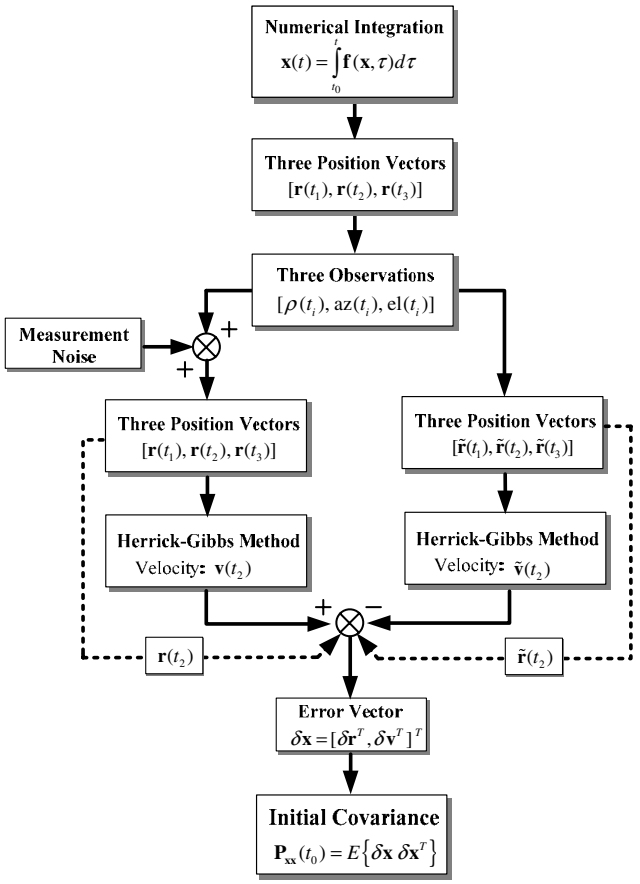

Fig. 2 Diagram for initialization for the state estimate and covariance matrix.

middle velocity vector $\boldsymbol{v}_2$ at time t_2 is obtained by applying the HG algorithm (see [12] for details):

$$\boldsymbol{v}_2 = -\Delta t_{32}\left(\frac{1}{\Delta t_{21}\Delta t_{31}} + \frac{\mu}{12r_1^3}\right)\boldsymbol{r}_1 + (\Delta t_{32} - \Delta t_{21})\left(\frac{1}{\Delta t_{21}\Delta t_{32}} + \frac{\mu}{12r_2^3}\right)\boldsymbol{r}_2 + \Delta t_{21}\left(\frac{1}{\Delta t_{32}\Delta t_{31}} + \frac{\mu}{12r_3^3}\right)\boldsymbol{r}_3 \tag{50}$$

where $\Delta t_{ij} = t_i - t_j$. For generating an error state covariance matrix, a Monte Carlo simulation method can be used. The calculated state information obtained from the HG has errors inherently due to the approximation used in the algorithm. Subtracting the calculated position and velocity vector $\hat{\boldsymbol{x}}_0 = [\tilde{\boldsymbol{r}}(t_2)\tilde{\boldsymbol{v}}(t_2)]$ from the reference state vector $\boldsymbol{x}_0 = [\boldsymbol{r}(t_2)\boldsymbol{v}(t_2)]$ provides the state error vector $\delta\boldsymbol{x}_0$, and the error covariance $\boldsymbol{P}_0$ is formulated by using the Monte Carlo runs:

$$\boldsymbol{P}_0 = \frac{1}{N_m - 1}\sum_{i=1}^{N_m}[\boldsymbol{x}_0^{(i)} - \hat{\boldsymbol{x}}_0^{(i)}][\boldsymbol{x}_0^{(i)} - \hat{\boldsymbol{x}}_0^{(i)}]^T \tag{51}$$

where N_m is the number of the Monte Carlo simulation runs, and $\hat{\boldsymbol{x}}_0^{(i)}$ and $\boldsymbol{x}_0^{(i)}$ are the ith state vectors obtained from the HG algorithm, respectively. The Monte Carlo simulation is accomplished by using different noisy observations for each simulation, and the procedure is illustrated in Fig. 3. This procedure for the initial covariance obviously could not be used in the real world as truth is not known.

VI. Filtering Performance Analysis

To check the performance of the proposed nonlinear filters in terms of state estimate optimality, two systematic methods are introduced.

A. Optimality Analysis

Optimality of the nonlinear filtering guarantees that the state estimation errors from the actual trajectory are small (the model estimates are unbiased) and the residuals consistent with their predicted statistics [3]. However, truncated errors due to the neglected terms in the approximation of the nonlinear models can cause biased estimation resulting in large estimation errors. Thus, measuring the estimate residuals and consistency with their statistics is an alternative way for checking the filtering optimality. For this analysis a simple, but efficient, methodology is introduced for the simulation study. First, the mean square error (MSE) of the estimate $\hat{\boldsymbol{x}}_k$ is defined as [15]

$$\mathrm{MSE}\{\Delta\boldsymbol{x}_k\} \triangleq E\{[\Delta\boldsymbol{x}_k - E\{\Delta\boldsymbol{x}_k\}][\Delta\boldsymbol{x}_k - E\{\Delta\boldsymbol{x}_k\}]^T\} \tag{52}$$

where the error vector $\Delta\boldsymbol{x}_k \equiv \boldsymbol{x}_k - \hat{\boldsymbol{x}}_k$ is given by the difference between the true state vector $\boldsymbol{x}_k$ and estimated state vector $\hat{\boldsymbol{x}}_k = \hat{\boldsymbol{x}}_k^+$. If the estimate is biased, then the mean square error is obtained as follows:

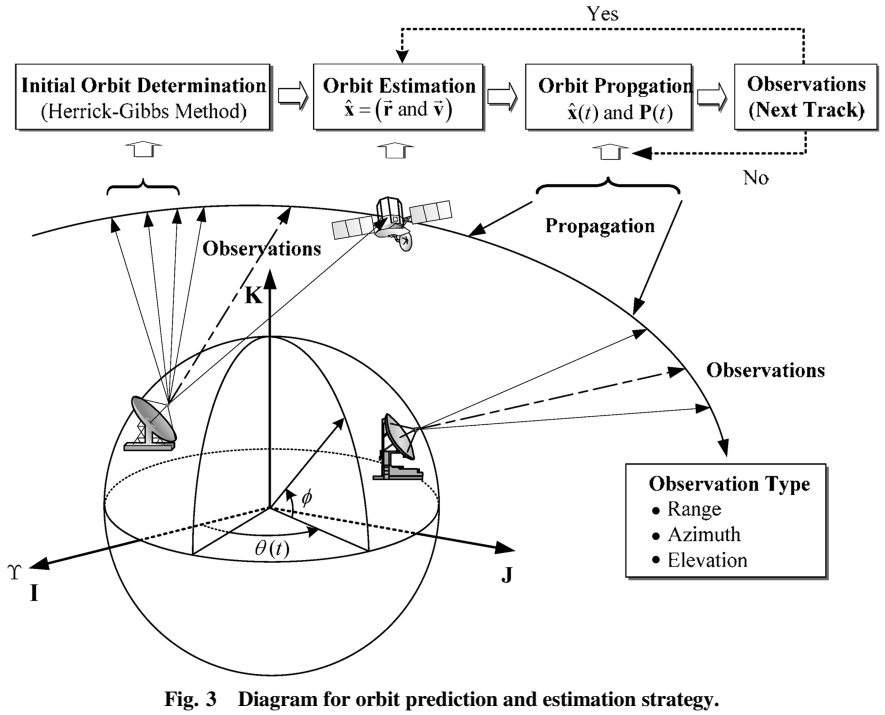

Fig. 3 Diagram for orbit prediction and estimation strategy.

$$\text{MSE}\{\Delta \boldsymbol{x}_k\} = \boldsymbol{P}_k - \boldsymbol{b}_k \boldsymbol{b}_k^T \tag{53}$$

where $\boldsymbol{b}_k$ is the bias obtained by taking the expected value of the estimate error, that is,

$$\boldsymbol{b}_k = E\{\Delta \boldsymbol{x}_k\} \tag{54}$$

When the estimate $\hat{\boldsymbol{x}}_k$ is not biased, the expected magnitude value of the errors is determined by the covariance

$$E\left\{\Delta \boldsymbol{x}_k \Delta \boldsymbol{x}_k^T\right\} = \boldsymbol{P}_k \tag{55}$$

Note that for unbiased estimate cases this reduces to the consistency analysis test [15]. Now, with the unbiased estimate assumption, the expectation of the quadratic value is obtained by

$$E\left\{\Delta \boldsymbol{x}_k^T \boldsymbol{A}_k \Delta \boldsymbol{x}_k\right\} = \text{tr}\left[\boldsymbol{A}_k E\left\{\Delta \boldsymbol{x}_k \Delta \boldsymbol{x}_k^T\right\}\right] = \text{tr}\left[E\left\{\Delta \boldsymbol{x}_k \Delta \boldsymbol{x}_k^T\right\} \boldsymbol{A}_k\right] \tag{56}$$

If the matrix $\boldsymbol{A}_k$ is the inverse covariance matrix $\boldsymbol{P}_k^{-1}$, then the mean value reduces to

$$E\{\Delta \boldsymbol{x}_k^T \boldsymbol{A}\, \Delta \boldsymbol{x}_k\} = \text{tr}[\boldsymbol{P}_k^{-1} \boldsymbol{P}_k] = \text{tr}[\boldsymbol{I}_n] = n \tag{57}$$

which means that the expected normalized error squared should be equal to n, the dimension of the random error vector. This fact can be used to check a degree of optimality or consistency in the update of the state and covariance used in various filters and estimators.

For this analysis, the optimality index τ_k based on the mean square error is defined as

$$\tau_k \equiv \frac{1}{\sqrt{n}} \{[\boldsymbol{x}_k - \hat{\boldsymbol{x}}_k]^T \boldsymbol{P}_k^{-1} [\boldsymbol{x}_k - \hat{\boldsymbol{x}}_k]\}^{1/2} \tag{58}$$

where $\boldsymbol{P}_k^{-1}$ is the updated covariance matrix. If the value of the optimality index τ_k is much greater than unity, then the effect of the nonlinearity due to the neglected terms is severe, but in contrast if τ_k is close to unity, we can assume that the nonlinearity from the linearization is negligible. Thus, these conditions can indicate both the optimality of the performance of the nonlinear filters and the nonlinearity due to neglected terms. If nonlinear filters produce unbiased estimates with consistent covariances, then the estimated results should make the optimality index close to unity.

B. Estimation Error Outlier

In this study, the average rms error is used for the quantitative performance criterion of the proposed filters. The rms error $\delta \boldsymbol{x}_i$ of the state vector component is defined by

$$\delta \boldsymbol{x}_i = \sqrt{\frac{1}{N_m} \sum_{j=1}^{N_m} [x_{i,j}(k) - \hat{x}_{i,j}(k)]^2} \tag{59}$$

where N_m is the number of Monte Carlo runs, the subscript j denotes the jth simulation run, and i represents the ith component of the state vector $\boldsymbol{x}(k)$ and its current estimate vector $\hat{\boldsymbol{x}}(k)$. The criteria for judging the performance of the proposed nonlinear filters are the magnitude of the residuals and their statistics. If the measurement residuals or the state estimation errors are sufficiently small and consistent with their statistics, then the filter is trusted to be operating consistently. In other words, the most common way for testing the consistency of the filtering results is to depict the estimated state errors with the three-sigma bound given by $\pm 3\sqrt{\boldsymbol{P}_k^{+}}$. If the errors lie within the bound, the estimation result is assumed to be consistent and reliable. Instead of the state estimation errors, the measurement innovation vector can be also used for the filter performance analysis. If the measurement residuals lie within the two-sigma bound, $\pm 2\sqrt{\boldsymbol{P}_{k+1}^{vv}}$, it indicates the 95% confidence of the estimation results.

VII. Simulation Results

In this section the performance of the proposed nonlinear filters, the EKF, DDF, and UKF, is demonstrated through simulation examples using realistic satellite and observation models. The satellite under consideration has the following orbit parameters: $a = 6778.136$ km, $e = 1.0 \times 10^{-5}$, $i = 51.6$ deg, $\omega = 30$ deg, $\Omega = 25$ deg, $B_C = 1.0 \times 10^8$ kg/km^2. The system dynamic equations consist of the two-body motion, J_2 zonal perturbation and drag perturbation. All dynamic and matrix differential equations are numerically integrated by using a fourth-order Runge–Kutta algorithm. One ground tracking site was used to take observations and the location of the sensor was selected to be Eglin Air Force Base, whose location is at 30.2316 deg latitude and 86.2147 deg west longitude. Each observation consists of range, azimuth, and elevation angles, and the measurement errors were considered to be Gaussian random processes with zero means and variances:

$$\begin{gathered} \sigma_{\text{range}} = 25.0 \text{ m}, \qquad \sigma_{\text{azimuth}} = 0.015 \text{ deg} \\ \sigma_{\text{elevation}} = 0.015 \text{ deg} \end{gathered} \tag{60}$$

In the simulation studies the initial position and velocity estimates and covariance for the EKF and SPFs (UKF, DDF) are obtained using the Herrick–Gibbs algorithm as discussed earlier. The "solve-for" state vector $\boldsymbol{x}_k = [\boldsymbol{r}_k^T \boldsymbol{v}_k^T]^T \in \Re^n$ consists of the position and velocity components in the first track estimation. The state vector for the UKF is augmented with the process and measurement noise terms, $\boldsymbol{x}_k^a = [\boldsymbol{x}_k^T \boldsymbol{w}_k^T \boldsymbol{v}_k^T]^T \in \Re^{n+q+l}$. The parameters used in the UKF are the scaling factors associated with the scaled unscented transformation. $\beta = 2$ is set to capture the higher-order (fourth) terms in the Taylor-series expansion and $\alpha = 10^{-3}$ is chosen to make the sample distance independent of the state size. The interval length $h = \sqrt{3}$ is set for a Gaussian distribution in the DDF.

A. First Track Estimation

The state vector $\boldsymbol{x}_k = [x, y, z, \dot{x}, \dot{y}, \dot{z}]^T$ consists of the position and velocity components. Note that the drag coefficient was not estimated in the first track because we do not have enough data for the estimation of the coefficient, and this is based on the assumption that the drag effect is negligible due to the short track length.

The true initial values $\boldsymbol{x}_0$ of the state variables for the simulation study were

$$\begin{aligned} x_0 &= 4011.5713 \text{ km}, & y_0 &= 4702.6493 \text{ km} \\ z_0 &= 3238.3582 \text{ km} & \dot{x}_0 &= -5.653084 \text{ km/s} \\ \dot{y}_0 &= 1.5401902 \text{ km/s}, & \dot{z}_0 &= 4.7765408 \text{ km/s} \end{aligned} \tag{61}$$

For the nominal reference trajectory, the following initial estimates $\hat{\boldsymbol{x}}_0$ were used:

$$\begin{aligned} \hat{x}_0 &= 3931.3399 \text{ km}, & \hat{y}_0 &= 4608.5963 \text{ km} \\ \hat{z}_0 &= 3173.5911 \text{ km} & \hat{\dot{x}}_0 &= -5.540022 \text{ km/s} \\ \hat{\dot{y}}_0 &= 1.5093864 \text{ km/s}, & \hat{\dot{z}}_0 &= 4.6810100 \text{ km/s} \end{aligned} \tag{62}$$

The initial covariance $\boldsymbol{P}_0 \in \Re^{6\times 6}$ used for the filters resulted from simulations of the Herrick–Gibbs method and has diagonal elements with position variances of 10^{-1} km^2, and velocity variances equal to 5×10^{-4} km^2/s^2.

$$\begin{aligned} &\boldsymbol{P}_0 \\ &= \text{diag}([\,10^{-1} \quad 10^{-1} \quad 10^{-1} \quad 5\times 10^{-4} \quad 5\times 10^{-4} \quad 5\times 10^{-4}\,]) \end{aligned} \tag{63}$$

Often, the process noise for the dynamic model errors is added to the acceleration terms to help adjust the convergence properties. In this study, however, the value for $\boldsymbol{Q}(t)$ is set, rather than adjusted, to model the realistic environment as close as possible. For instance, the acceleration due to J_2 is approximately 10^{-5} km/s^2 and the truncated

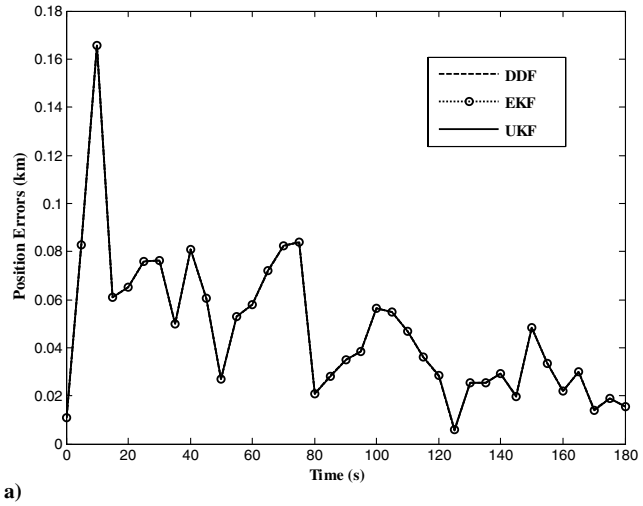

a)

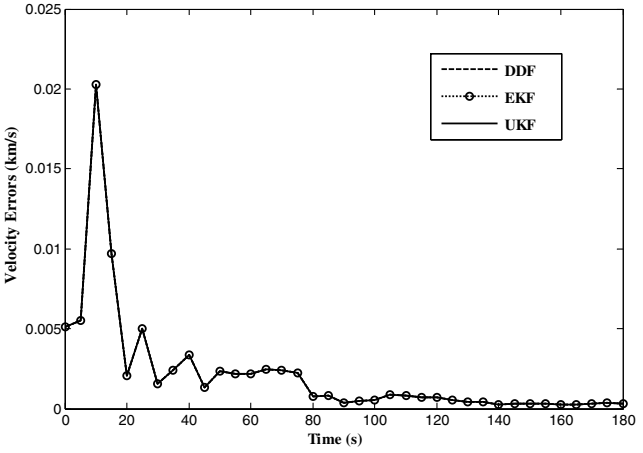

b)

Fig. 4 a) Absolute magnitude of position errors with initial estimates from Herrick–Gibbs method; b) absolute magnitude of velocity errors with initial estimates from Herrick–Gibbs method.

or ignored perturbing accelerations are considered to be of $\mathcal{O}(J_2^2)$; thus the process noise covariance matrix for the low-earth orbit scenario model is

$$\boldsymbol{Q}(t) = \text{diag}([0 \quad 0 \quad 0 \quad 10^{-16} \quad 10^{-16} \quad 10^{-16}])\ \text{km}^2/\text{s}^2 \quad (64)$$

Note that because the process noise covariance $\boldsymbol{Q}(t)$ comes from a continuous-time dynamic system model, it is necessary to convert it into the discrete-time form of the covariance $\boldsymbol{Q}_k$ through an approximate numerical integration scheme [13], using first-order approximation, $\boldsymbol{Q}_k \approx \boldsymbol{Q}(t)\Delta t$, where Δt is the time step in the propagation step.

The simulation results shown in Figs. 4a and 4b indicate the average magnitude of the position and velocity estimate errors generated by each filter through a Monte Carlo simulation consisting of 30 runs. As can be seen, no advantage of the SPFs (UKF, and DDF) over the EKF in the first track is evident, which indicates that the effect of any nonlinearity on the filters is negligible with the small initial state errors along with the small process noises over the short track length. This is the expected result because setting $\boldsymbol{Q}(t)$ to zero in both filters should obtain theoretically similar results with the sequential estimation for the state and covariance. The earlier estimation results can be verified by employing the optimality and/or consistency index τ_k. Figure 5 shows the plot of the optimality measure taken in the state estimation. The plots from the nonlinear filters, the EKF and the SPFs, exhibit similar performance with a value close to unity, which indicates that the neglected higher-order terms in the nonlinear filtering algorithms are not severe and all the

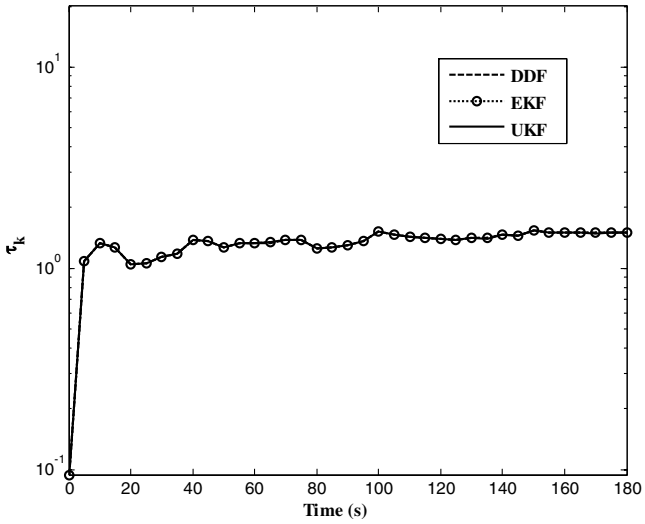

Fig. 5 Optimal and consistency test for nonlinear state estimation in first track estimation.

filters are producing near-optimal accurate estimates with small biased errors.

In the next simulation, the values of the process and initial state covariance matrices are increased to check the robustness of the filters. In these simulations, $\mathcal{P}_0 = k_P \boldsymbol{P}_0$ and $\mathcal{Q}(t) = k_Q \boldsymbol{Q}(t)$ are used, where $k_P = 10^2$ and $k_Q = 10^9$, respectively. The results are shown in Figs. 6a and 6b. The better performance of the UKF is very clear, particularly when comparing to Fig. 4, in which the results of the UKF, DDF, and EKF were essentially identical. This indicates that the UKF is less sensitive than the DDF and EKF to the variation of the initial covariance, and is robust to the large system uncertainties. This means that the tuning of the UKF is easier than that of the EKF. These simulation results provide a key indicator that the UKF can play a role in real-time orbit determination when there are large initial estimate uncertainties in the system models. Note that if the system dynamic models have large modeling errors, the performance of the UKF should be more obvious.

To further check the sensitivity of the filters to initial errors, large initial errors are set, but the same initial covariance matrices in Eqs. (63) and (64) are used. The simulation results shown in Figs. 7a and 7b illustrate the orbit estimation with large initial errors. These figures clearly show the superior performance of the DDF and UKF over the EKF. The EKF position and velocity estimate errors are decreasing, but converge to errors that are at least twice those of the DDF and UKF. The UKF and the DDF converge continuously and fast with smaller errors, which indicates that they are performing in a near-optimal fashion. The performance of the UKF and the DDF are similar in the case of the large initial error, but the DDF is slightly superior to the UKF. This contrasts with the case with large initial covariances in which the UKF performance was better than the DDF. Figure 8 is the plot of the range measurement innovation error with the two-sigma bound when the initial state estimates have large errors. The range innovations errors obtained from the UKF and the DDF vary inside the sigma bound, but the range residual from the EKF lies outside the boundary with large errors indicating suboptimal performance.

B. Second Track Estimation

We now consider the estimation with multiple tracks that have a 24-h separation. First, the estimated states and updated covariance matrix obtained from the first track estimation are propagated using each propagation method to the next available track. For the covariance propagation the Lyapunov equation is used for the EKF, the scaled unscented transformation (SUT) is used for the UKF, and the compound matrices containing divided differences are used in the DDF. Each propagation method gives a different level of the accuracy. The first-order nonlinear filter, the EKF, has the same

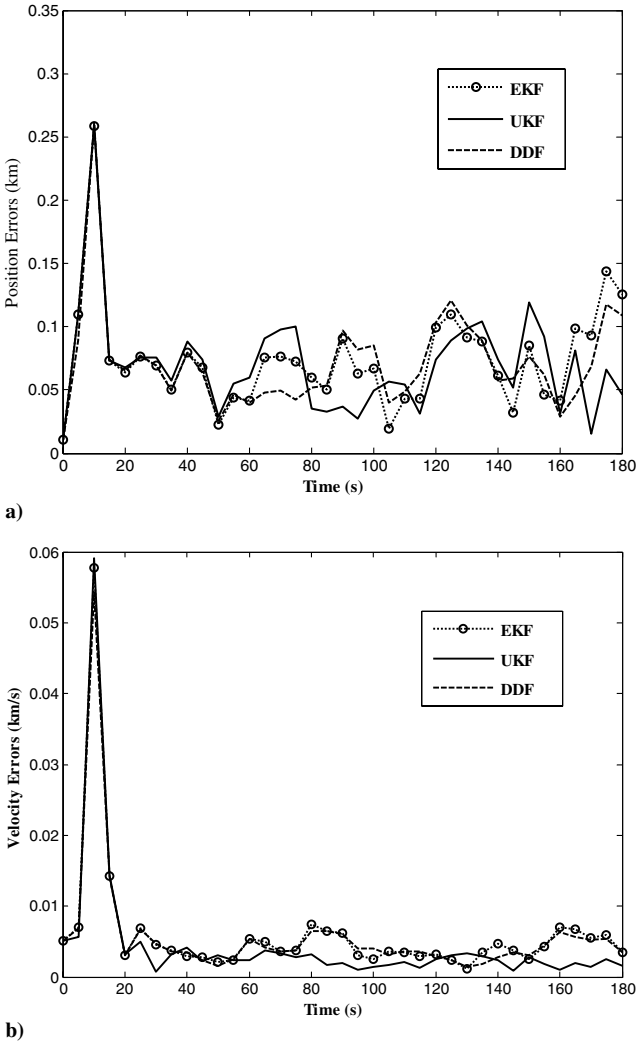

Fig. 6 a) Absolute magnitude of position errors with large system uncertainty errors; b) absolute magnitude of velocity errors with large system uncertainty errors.

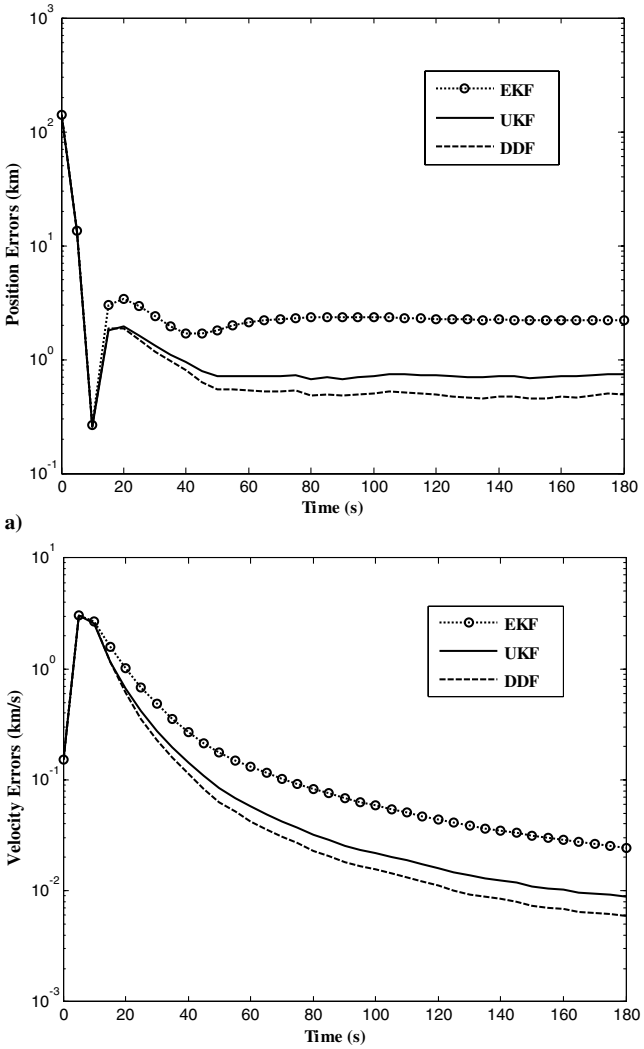

Fig. 7 a) Absolute magnitude of position errors with large initial errors; b) absolute magnitude of velocity errors with large initial errors.

approximation accuracy up to the first-order Taylor-series expansion. The UKF and the DDF also have the identical state propagation accuracy, but they have slightly different propagation accuracy for the covariance. Both the UKF and DDF filters, however, result in approximations accurate up to the third order of the Taylor-series expansion for a Gaussian distribution. The true and estimated states from the first track are also propagated using each dynamic model until the first observation of the second track is available. Therefore, the inputs to the orbit determination in the second track are the initial state errors and covariance matrix of states propagated from the end of the first track. If the separation between the tracks becomes longer, the inputs of the propagated state and covariance have larger errors. From the experience in the previous simulation examples superior, performance results of the UKF and the DDF should be obtained over the first-order nonlinear filter.

The state vector $\boldsymbol{x}_k = [x, y, z, \dot{x}, \dot{y}, \dot{z}, C_d]^T$ consists of the position, velocity, and the drag coefficient components. The true initial values $\boldsymbol{x}_0$ of the state variables for the simulation study were

$$x_0 = 5064.2972 \text{ km}, \qquad y_0 = 4058.0902 \text{ km}$$
$$z_0 = 2563.8776 \text{ km} \qquad \dot{x}_0 = -4.769793 \text{ km/s}$$
$$\dot{y}_0 = 2.6472337 \text{ km/s}, \qquad \dot{z}_0 = 5.2366325 \text{ km/s}, \qquad C_d = 2.0 \tag{65}$$

For the nominal reference trajectory, the following initial estimates $\hat{\boldsymbol{x}}_0$ were used:

$$\hat{x}_0 = 4916.4981 \text{ km}, \qquad \hat{y}_0 = 4136.0481 \text{ km}$$
$$\hat{z}_0 = 2721.4771 \text{ km} \qquad \hat{\dot{x}}_0 = -4.946330 \text{ km/s}$$
$$\hat{\dot{y}}_0 = 2.5016529 \text{ km/s}, \qquad \hat{\dot{z}}_0 = 5.1424392 \text{ km/s}, \qquad \hat{C}_d = 3.5 \tag{66}$$

The state covariance $\boldsymbol{P}_0 \in \Re^{6\times 6}$ for the filters in the second track estimation was obtained by propagating the output covariance matrix at the end of the first track estimation, and the variance of the drag coefficient was set $\sigma^2_{C_d} = 0.5$. Thus, the estimated C_D is approximately a 2σ value. The same process noise covariance matrix $\boldsymbol{Q}(t)$ was used as in the first track estimation.

Figures 9a and 9b depict the estimation of the states (position and velocity) in the second track with a 3-min track separated from the first track by 24 h. In the results, the qualitative observation is made that the UKF and the DDF show far better performance in the state estimation over the EKF when the tracks are separated for multiple orbits with sparse measurement data. It can also be observed how quickly the UKF and the DDF converge to the true state of the system. The degradation of the EKF performance is related to the fact that the length of tracking necessary for the filters to get the accurate solutions is short, and the covariance prediction for a long time interval leads to inaccurate predictions errors due to the effects of the neglected nonlinear terms. Even more encouraging, the UKF is showing the best performance among the filters. This agrees well with our expectations and indicates that the higher-order terms are

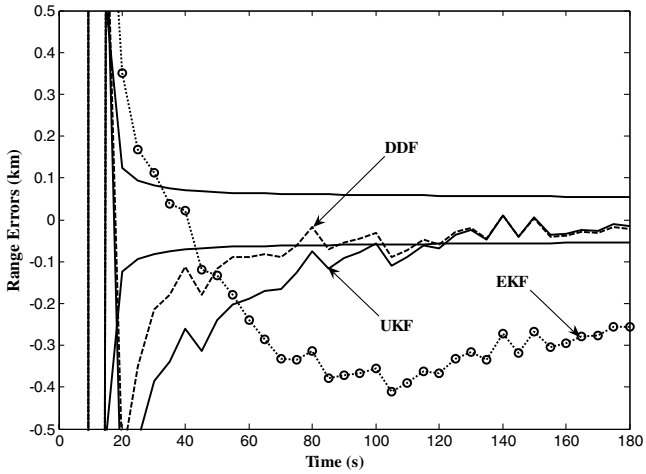

Fig. 8 Range measurement innovation errors with two-sigma outliers.

necessary to capture the large initial condition errors adequately. These higher-order terms also aid in the accurate estimation of the state and covariance in the case. In Fig. 10, the absolute magnitude values of the drag coefficient errors are depicted in the second-track estimation. The performance of the parameter estimation among the nonlinear filters is not obvious. All the nonlinear filters generated decreasing error solutions, but converged solutions. The advantage

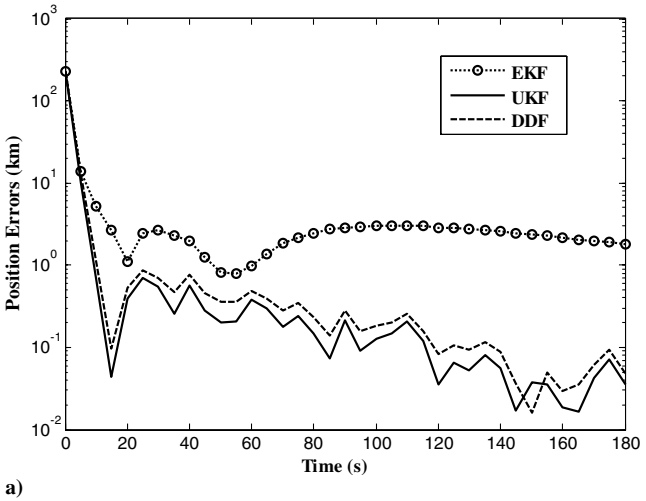

a)

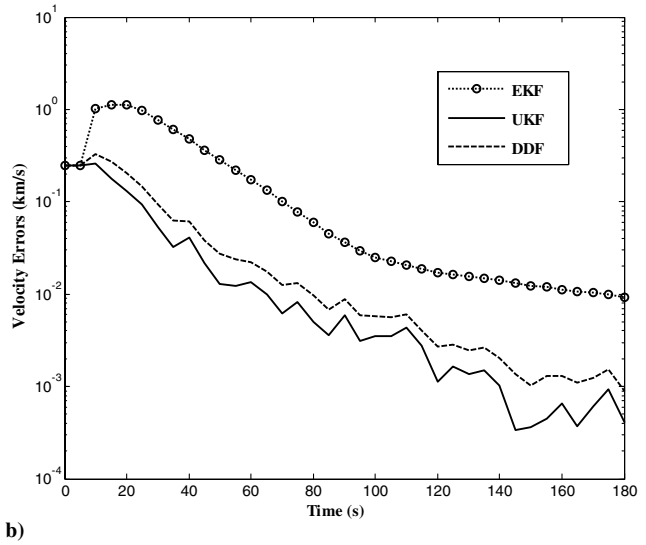

b)

Fig. 9 a) Absolute magnitude of position errors in second track estimation; b) absolute magnitude of velocity errors in second track estimation.

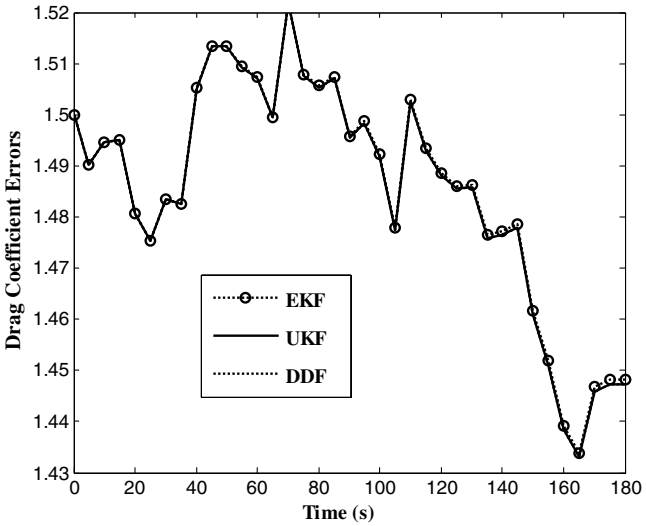

Fig. 10 Absolute magnitude of drag coefficient errors in second track estimation.

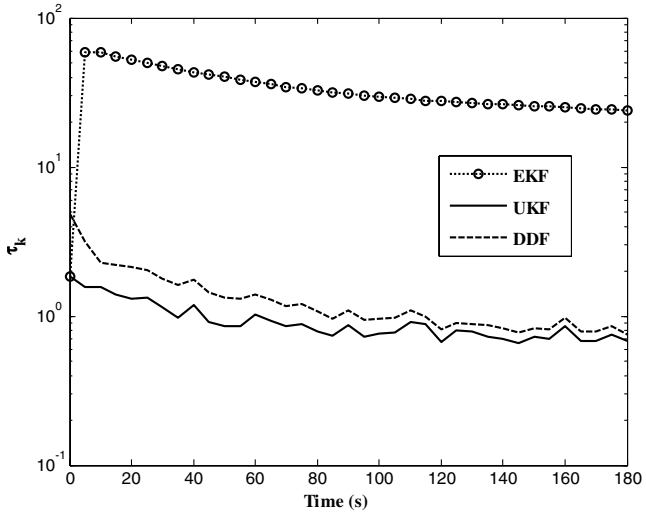

Fig. 11 Optimality and consistency test for nonlinear state estimation in second track estimation.

of the SPFs in the drag coefficient estimate in the second track is not obvious over the EKF.

Figure 11 shows the optimality (consistency) measure in the second track state and parameter estimation from the proposed nonlinear filters. The optimality index obtained from the higher-order nonlinear filters, the SPFs, remained close to the unity, but the optimality index from the EKF varies with large deviations. This indicates that the SPFs exhibit similar near-optimal performance and successfully compensate for the neglected nonlinearities due to approximation, but the first-order nonlinear filter, the EKF, failed to compensate for the neglected errors.

According to the criteria of the rms errors, and the optimality and consistency test, and the innovation errors presented so far, it is seen that the performance of the SPFs is near optimal in the sense that they compensate for the neglected modeling errors due to the linearization step as well as the unknown system uncertainties, primarily the atmospheric drag uncertainty.

VIII. Conclusions

In this paper new nonlinear filtering algorithms, called sigma point filters, that include the unscented Kalman filter and the divided difference filters are used to obtain accurate and efficient orbit estimation. In addition, an efficient method to measure the dynamic

and measurement nonlinearities of the proposed filters is introduced. Simulation results indicate that the performances of the unscented Kalman filter and the second-order divided difference filter are similar, but superior to both the standard extended Kalman filter and the first-order divided difference filter in terms of the estimate accuracy and sensitivity to large initial errors. In particular, the robustness of the unscented Kalman filter to the initial covariance matrices makes it easy to tune the filter and the sigma point filters provide the flexibility of implementation without the derivation of Jacobian and Hessian matrix. The advantages of the proposed nonlinear filtering algorithms make these suitable for efficient nonlinear estimation in not only real-time satellite orbit determination but also other application areas.

Acknowledgment

This work was supported by the Texas ARP/ATP Program Grant under the project contract No. 000512-0343-2001.

References

[1] Alfriend, K. T., "A Dynamic Algorithm for the Processing of UCTs," *Proceedings of the AAS/AIAA Astrodynamics Specialist Conference*, Vol. 97, Univelt, San Diego, CA, 1998, pp. 123–131.

[2] Alfriend, K. T., Akella, M. R., Frisbee, J., Foster, J. L., Lee, D.-J., and Wilkins, M. P., "Probability of Collision Error Analysis," *Space Debris*, Vol. 1, No. 1, 1999, pp. 21–35.

[3] Jazwinski, A. H., *Stochastic Processes and Filtering Theory*, Academic Press, New York, 1970.

[4] Julier, S. J., Uhlmann, J. K., and Durrant-Whyte, H. F., "A New Approach for Filtering Nonlinear Systems," *Proceedings of the American Control Conference*, IEEE, New York, 1995, pp. 1628–1632.

[5] Julier, S. J., Uhlmann, J. K., and Durrant-Whyte, H. F., "A New Method for Nonlinear Transformation of Means and Covariances in Filters and Estimators," *IEEE Transactions on Automatic Control*, Vol. 45, No. 3, March 2000, pp. 477–482.

[6] Schei, T. S., "A Finite-Difference Method for Linearization in Nonlinear Estimation Algorithms," *Automatica*, Vol. 33, No. 11, Nov. 1997, pp. 2053–2058.

[7] Norgaard, M., Poulsen, N. K., and Ravn, O., "New Developments in State Estimation for Nonlinear Systems," *Automatica*, Vol. 36, No. 11, Nov. 2000, pp. 1627–1638.

[8] Ito, K., and Xiong, K., "Gaussian Filters for Nonlinear Filtering Problems," *IEEE Transactions on Automatic Control*, Vol. 45, No. 5, May 2000, pp. 910–927.

[9] Lee, D.-J., and Alfriend, K. T., "Adaptive Sigma Point Filtering for State and Parameter Estimation," *AIAA/AAS Astrodynamics Specialist Conference and Exhibit*, AIAA Paper 2004-5101, Aug. 2004.

[10] van der Merwe, R., Wan, E. A., and Julier, S. J., "Sigma-Point Kalman Filters for Nonlinear Estimation and Sensor Fusion: Applications to Integrated Navigation," *AIAA Guidance, Navigation, and Control Conference and Exhibit*, AIAA Paper 2004-5120, Aug. 2004.

[11] Lee, D.-J., and Alfriend, K. T., "Precise Real-Time Orbit Estimation Using the Unscented Kalman Filter," *Proceedings of AAS/AIAA Space Flight Mechanics Meeting*, Vol. 114, Univelt, San Diego, CA, 2003, pp. 1853–1872.

[12] Vallado, D. A., *Fundamentals of Astrodynamics and Applications*, McGraw–Hill, New York, 1997, Chap. 6.

[13] Wan, E. A., and van der Merwe, R., "The Unscented Kalman Filter," *Kalman Filtering and Neural Networks*, edited by S. Haykins, John Wiley & Sons, New York, 2001, Chap. 7.

[14] Hough, M. E., "Improved Performance of Recursive Tracking Filters Using Batch Initialization and Process Noise Adaptation," *Journal of Guidance, Control, and Dynamics*, Vol. 22, No. 5, 1999, pp. 675–681.

[15] Bar-Shalom, Y., Li, X.-R., and Kirubarajan, T., *Estimation with Applications to Tracking and Navigation*, John Wiley & Sons, New York, 2001.

C. McLaughlin
Associate Editor